The Journal of Chemical Physics

Hydration dynamics of a lipid membrane: Hydrogen bond networks and lipid-lipid associations

Cite as: J. Chem. Phys. **148**, 094901 (2018); https://doi.org/10.1063/1.5011803
Submitted: 03 November 2017 . Accepted: 10 February 2018 . Published Online: 01 March 2018

Abhinav Srivastava, and Ananya Debnath

Hydration dynamics of a lipid membrane: Hydrogen bond networks and lipid-lipid associations

Abhinav Srivastava and Ananya Debnath[a)]
Department of Chemistry, Indian Institute of Technology Jodhpur, Karwad, Rajasthan, India

(Received 3 November 2017; accepted 10 February 2018; published online 1 March 2018)

Dynamics of hydration layers of a dimyristoylphosphatidylcholine (DMPC) bilayer are investigated using an all atom molecular dynamics simulation. Based upon the geometric criteria, continuously residing interface water molecules which form hydrogen bonds solely among themselves and then concertedly hydrogen bonded to carbonyl, phosphate, and glycerol head groups of DMPC are identified. The interface water hydrogen bonded to lipids shows slower relaxation rates for translational and rotational dynamics compared to that of the bulk water and is found to follow sub-diffusive and non-diffusive behaviors, respectively. The mean square displacements and the reorientational auto-correlation functions are slowest for the interfacial waters hydrogen bonded to the carbonyl oxygen since these are buried deep in the hydrophobic core among all interfacial water studied. The intermittent hydrogen bond auto-correlation functions are calculated, which allows breaking and reformations of the hydrogen bonds. The auto-correlation functions for interfacial hydrogen bonded networks develop humps during a transition from cage-like motion to eventual power law behavior of $t^{-3/2}$. The asymptotic $t^{-3/2}$ behavior indicates translational diffusion dictated dynamics during hydrogen bond breaking and formation irrespective of the nature of the chemical confinement. Employing reactive flux correlation analysis, the forward rate constant of hydrogen bond breaking and formation is calculated which is used to obtain Gibbs energy of activation of the hydrogen bond breaking. The relaxation rates of the networks buried in the hydrophobic core are slower than the networks near the lipid-water interface which is again slower than bulk due to the higher Gibbs energy of activation. Since hydrogen bond breakage follows a translational diffusion dictated mechanism, chemically confined hydrogen bond networks need an activation energy to diffuse through water depleted hydrophobic environments. Our calculations reveal that the slow relaxation rates of interfacial waters in the vicinity of lipids are originated from the chemical confinement of concerted hydrogen bond networks. The analysis suggests that the networks in the hydration layer of membranes dynamically facilitate the water mediated lipid-lipid associations which can provide insights on the thermodynamic stability of soft interfaces relevant to biological systems in the future. *Published by AIP Publishing.*
https://doi.org/10.1063/1.5011803

I. INTRODUCTION

The hydration of a bilayer plays a crucial role in determining the function of cell membranes by affecting their integrity and dynamics. Water near biological molecules such as proteins, membranes, and DNA are commonly known as "biological water,"[1] and their behaviors are remarkably different than the bulk water (BW).[2–4] Though the structure and dynamics of biological water have been investigated significantly using both experiments and computer simulations, several questions regarding the origin of slow relaxation rates of hydration layers of membranes are unresolved to date. It is not clear whether different chemical moieties of lipid heads or chemical influence on hydrogen bond networks significantly slow down the relaxation rates. Whether the degree of slowing down of the relaxation is dependent on the chemical nature of the confinement is not investigated. The relation between slow rotational and translational relaxation rates of chemically confined water near bilayer and dynamic heterogeneity is not thoroughly established yet. Whether the nature of the hydrogen bond relaxation rate is thermodynamics or kinetic is not known for the hydration layer of bilayers. The present work attempts to answer these questions and unravels their implications on membrane associations and other biomolecules.

Vibrational anisotropic experiments are used to probe the anisotropy of water in a multi-bilayer as a function of lipid hydration level since the water stretching mode is dependent on the local environment.[5] A pioneering 2D infrared (2D-IR) spectroscopy experiment on water directly characterizes the mechanism of hydrogen bond network rearrangement[6,7] by probing the OH frequency time evolution. However, the 2D-IR cannot distinguish between the formation of a hydrogen bond with and without allowing the change of partners. Polarization-resolved 2D-IR experiments are successful in measuring the reorientation associated with the hydrogen bond exchange.[8] Although linear or 2D infrared spectroscopy[9–11] provides information on the hydrogen bond dynamics and pump-probe spectroscopy provides data on vibrational

[a)]Electronic mail: ananya@iitj.ac.in

relaxation and reorientational motion, limited spatial resolution, intermolecular coupling, energy transfer, non-Condon effects, and distributions in vibrational lifetime are few sources of ambiguous results.[12] Other experimental techniques such as quasi-elastic neutron scattering (QENS), terahertz spectroscopy, optical Kerr-effect spectroscopy, nuclear magnetic resonance (NMR), ultrafast IR spectroscopy, and di-electric relaxation have been used to study water dynamics. A major limitation of the experimental techniques is the coupling of contributions from hydration layer and bulk and limited to the individual reorientation mechanism.[13–16] NMR can also provide information on weighted average of reorientational relaxation time,[17–19] but not on different individual mechanisms. The other drawback of the experimental techniques is sensitivity issues on their concentration dependency.[14]

Molecular dynamics studies have been carried out to study several properties of lipid bilayers. A fully hydrated dimyristoylphosphatidylcholine (DMPC) bilayer has been studied using the SPC water model showing two types of lateral diffusive behavior: cage hopping and two-dimensional liquid.[20] Between two groups of DMPC molecules, stable charge associations are formed between positively and negatively charged groups of DMPC.[21] Diffusion of protons near DMPC is inhibited at a membrane surface.[22] Molecular dynamics simulations are carried out to model the creation of bilayer gaps, a common process in bilayer patterning.[23] Thermodynamic properties of a hydrogen bond can be obtained from the probability distribution of donor-acceptor pair in the first hydration shell of an electronegative atom.[24] The Gibbs free energy of hydrogen bonding at equilibrium is found to be independent of the environment in alcohol solutions with an entropic barrier.[25] Molecular dynamics of hydration layers of the membrane protein reveal additive contributions from the membrane and the proteins to the activation energies of water diffusion.[26] However, the surface of DNA duplex intrinsically weakly interacts with water and translationally more mobile in nature.[27] The 2D-IR study of hydration layers confined in reverse micelles shows the correspondence between spectral decomposition performed in experiments and spatial decomposition in simulations.[28] A mosaic water orientation has been found near zwitterionic lipids using vibrational sum frequency generation (VSFG) spectra.[29] Molecular dynamics of water near DMPC lipids show that 70% of DMPC molecules are linked via bridging water and the average geometry of hydrogen bonding to oxygens of lipid heads is planar trigonal instead of steric tetragonal.[21] The vibrational dynamics of water in the vicinity of anionic and cationic head groups of multibilayers reveal the difference in vibrational lifetime for different charge groups.[30] The sum-frequency generation spectroscopy study shows that lipid carbonyl groups stabilize the hydrogen bond networks with its up-oriented O–H groups.[31]

Here we emphasize on the dynamics of water in the locale of DMPC lipid bilayers hydrated with TIP4P/2005 water using an all atom molecular dynamics simulation. Although previous studies have found the influence of chemical environment near lipid heads,[21,27–32] none of the investigations (a) decouple the contribution of bulk and interface water (IW) towards hydrogen bonding, (b) report the mechanism which interface water molecules follow to form hydrogen bonds and their implications on lipid aggregations, and (c) investigate the dynamics of hydrogen bond networks. Unlike the previous approaches, the water molecules are characterized in terms of hydrogen bonding to the lipid heads when confined to the interface. This can clearly de-construct the contribution of bulk and interface as well as the influence of different chemical environments. Further the interface water molecules are classified into four categories in terms of hydrogen bonds among themselves and concertedly to either another set of hydrogen bonded water or to lipid head groups. Thus, the present analysis can probe the dynamics of hydrogen bond networks instead of the dynamics of a single hydrogen bond shown in earlier approaches.[32] Radial distribution functions (RDFs), mean square displacements (MSDs), reorientational correlation functions, and hydrogen bond autocorrelation functions (HBACFs) are calculated for the concerted hydrogen bond networks to show the influence of chemical confinements on their dynamics. Our calculations demonstrate that chemical confinements play a crucial role on the relaxation rates of hydrogen bond networks and suggest that the networks influence the water mediated lipid-lipid associations.

II. SIMULATION DETAILS

Molecular dynamics simulations are carried out for 128 DMPC molecules in the presence of 5743 TIP4P/2005 water molecules. Since the TIP4P/2005 water model correctly reproduces the water phase diagram and the dynamics of water,[33] it is used in our simulations. Force field parameters for DMPC are obtained using the Berger united atom force field.[34,35]

An NPT run is carried out for 100 ns with a 2 fs time step. The system is equilibrated at 308 K using the velocity rescaling method with a coupling constant of 0.5 ps. The pressure is maintained at 1 bar using semi-isotropic pressure coupling by Berendsen pressure coupling[36] with a coupling constant of 0.1 ps. Coulombic and van der Waals interactions were cut off at 1 nm. Long-range interactions are corrected using the particle mesh Ewald[37–39] method with a 4 nm grid size. Periodic boundary conditions are applied in all three directions. Next an NVT simulation is carried out for 1 ns with a 0.4 fs time step where the last 100 ps is analyzed for water dynamics. Parameters for temperature coupling, cutoff distances, and long range interactions are the same as in the previous NPT run. Trajectories are collected at every 10 fs. The simulation box length for the hydrated DMPC lipid is 6.24 nm along the x and y directions and 7.95 nm along the z direction.

To compare the dynamics of interfacial water with bulk water, a box of 851 TIP4P/2005 water molecules is simulated for 2 ns with a 2 fs time step in an NPT ensemble with the same set of parameters as in the hydrated DMPC. Next a NVT run is carried out for 100 ps with a 0.4 fs time step. The box length for BW is 3.69 nm along the x and y directions and 1.84 nm along the z direction. Trajectories are collected at every 10 fs. All simulations are carried out using Gromacs 4.6.5.[40–45]

III. RESULTS AND DISCUSSIONS

A. Classification of water regimes

Water molecules are classified based on their proximity from the bilayer head groups along the bilayer normal. The Z coordinate of oxygen atoms of water molecules which continuously reside within ±3 Å from the peak position of the nitrogen density of the lipid head for the entire production run is classified as interface waters (IWs) and shown in Fig. 1. A molecule residing in a specific layer at a given time step is labeled as 1 and if it is outside the layer, it is labeled as 0.[46,47] Thus, the molecules which continuously reside in a specific layer are classified as interface water, and in our simulation there are such 104 interface water. The interface water molecules are associated with oxygen atoms of carbonyl (CO), glycerol (Glyc.), and phosphate (PO) groups of lipids via hydrogen bonds. To find out the presence of hydrogen bonds, the widely accepted geometric criteria[48–51] are used: $R_{OO} < 3.5$ Å and $\theta_{HOO} < 30°$, where R_{OO} is the distance between donor and acceptor oxygen atoms and θ_{HOO} is the angle between $\vec{OO}$ and $\vec{OH}$ bond vectors. No water molecules are found which form hydrogen bonds with the choline group of lipid heads. Based on the formation of hydrogen bonds among themselves and with the three head groups of DMPC lipids (CO, Glyc., and PO), interfacial waters are further classified among four categories. If an IW molecule is solely hydrogen bonded with any other IW, it is termed as IW–IW. If these hydrogens bonded IW–IW are concertedly hydrogen bonded to the oxygen atom of CO, Glyc., or PO of the DMPC head at any single time step during the production run, they are termed as IW–CO, IW–Glyc., and IW–PO, respectively. This makes the molecules diffusive in nature since they are not hydrogen bonded for the entire simulation period. Among the hydrogen bonded interfacial waters, there are total 70 IW–IW, 80 IW–CO, 55 IW–Glyc., and 98 IW–PO water molecules which form hydrogen bonds at least once for the 100 ps production run. Radial distribution functions (RDFs) between oxygen atoms of respective bound interfacial water are calculated by normalizing volume and density. The RDF in Fig. 2(a) shows that the peaks for all interfacial water are higher than bulk water (termed as BW). The RDF between oxygen atoms of bound interfacial water and three head groups shown in Fig. 2(b) demonstrates the ordered behaviors of the IW–CO, the IW–Glyc., and the IW–PO water molecules for the second hydration shells in addition to the first hydration shells. The enhanced amplitudes of the RDF for different classes of IW compared to the BW [Fig. 2(a)] indicate their higher tendency to be in the first and second hydration shells of each other. The presence of more oxygens in the nearest neighbors of each other for the interface water consequently disrupts the tetrahedral structure of the hydrogen bond network in bulk and results in defects in the hydrogen bonding networks in the presence of lipid heads.[52]

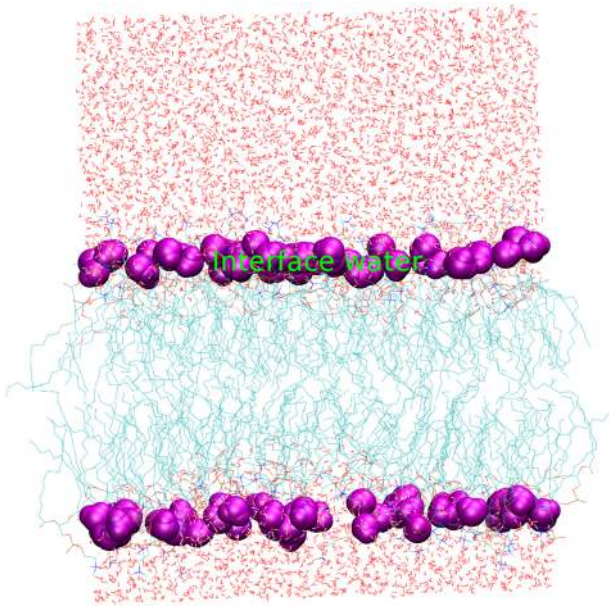

FIG. 1. DMPC bilayer in the presence of TIP4P/2005 water. Interfacial water is shown in magenta van der Waals (VDW) representation.[53]

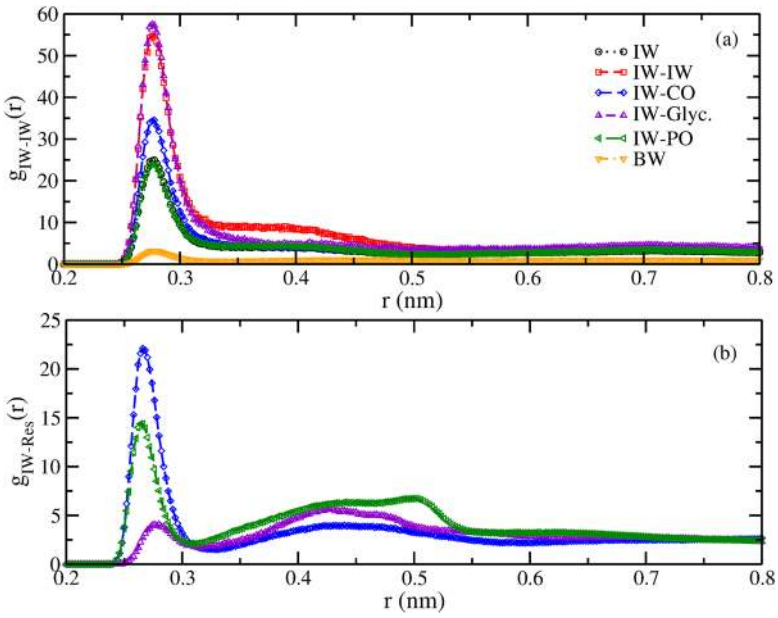

FIG. 2. Oxygen-oxygen RDF for different classes of water hydrogen bonded to (a) another water and (b) to lipid head groups (IW-Res). For the sake of clarity in the differences in amplitudes, the RDF of the interface water is not shown until they reach the values of bulk water.

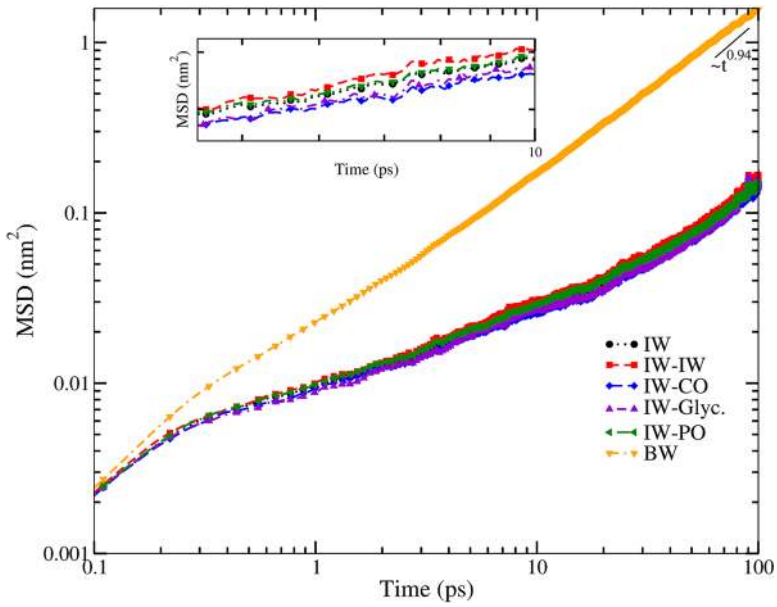

FIG. 3. Translational MSD for interfacial and bulk water where the BW has a diffusive regime and others follow a sub-diffusive behavior. Inset: MSD for interfacial waters showing slowest motion for IW–CO and fastest motion for IW–IW.

B. Translational mean square displacement

To quantify dynamical properties of water in different regimes, we computed the translational mean square displacement (MSD) for all classes of water discussed above using the following equation:

$$\langle r^2(t)\rangle = \frac{1}{N}\sum_{i=1}^{N}\langle[r_i(t+t') - r_i(t')]^2\rangle_{t'}, \quad (1)$$

where N is the total number of water molecules, t′ is the time origin, and t is the time difference. The angular bracket denotes the average over time origins. The translational MSD for different classes of water regimes is shown in Fig. 3. All classes of IW show a glass-like behavior from 0.2 to 1 ps after the ballistic region. At longer time, they obey power law function At^{α} where α depicts the type of diffusion. The values of α for four classes of interfacial water as well as the IW which are just confined to the interface and may or may not be hydrogen bonded are presented in Table I. All interfacial water molecules follow a sub-diffusive behaviour due to the geometric and chemical confinement at the interface forming hydrogen bonds among themselves or with the lipid heads. Interestingly, the MSD of the IW–CO or the IW–Glyc. is slower[54] than that of the IW–PO which is again slower than that of the IW–IW hydrogen bonded only among themselves (shown in the inset of Fig. 3). The slow translational diffusion of IW–CO/Glyc. are buried in the deeper region of lipid chains and translational motion are more restricted. The BW follows a diffusive behavior ($\alpha \approx 1$) for 60-90 ps. The value of the diffusion coefficient (D) for the BW is 2.49×10^{-5} cm^2 s^{-1} (Table I) which agrees well with the reported diffusion constant of 2.6×10^{-5} cm^2 s^{-1} for TIP4P/2005 water at 308 K.[55]

TABLE I. Values of α and diffusion coefficient (D) for translational MSD fitted with function At$^{\alpha}$. Correlation coefficients for all cases were >0.99.

Region	α	10^9D (m^2 s^{-1})
IW	0.51	
IW–IW	0.53	
IW–CO	0.45	
IW–Glyc.	0.53	
IW–PO	0.51	
BW	0.94	2.49 ± 0.31

C. Reorientational auto-correlation function (RACF)

To characterize rotational dynamics of water, we computed reorientational auto-correlation function (RACF) for all classes of water. The lth order Legendre polynomial of water reorientation is given by the following equation:

$$C_{vl}(t) = \frac{\langle\sum_{i=1}^{N} P_l[e_i^v(t).e_i^v(0)]\rangle}{\langle\sum_{i=1}^{N} P_l[e_i^v(0).e_i^v(0)]\rangle}, \quad (2)$$

where $e_i^v(t)$ is the vector for which the RACF is calculated and P_l is the lth order Legendre polynomial. We computed $C_{vl}(t)$ for the first and second order Legendre polynomial for vector normal to the plane of OHH ($\hat{n}$), OH bond vector ($\vec{OH}$), HH bond vector ($\vec{HH}$), and dipole moment vector $\vec{\mu}$. Figures 4 and 5 show the RACF for the interface and the bulk water for the first and second order Legendre polynomials (l = 1 and l = 2), respectively. Figures 4 and 5(a)–5(d) represent the RACF of $\hat{n}$, $\vec{OH}$, $\vec{HH}$, and $\vec{\mu}$, respectively. The RACF of the bulk water of all cases decays much rapidly to zero than all classes of IW showing no preferences in orientations. The RACF for the IW–IW and all IW overlaps with each other showing no differences in orientations when they are hydrogen bonded among themselves or not. For all the cases, the second order reorientation relaxations are more rapid than the first order relaxations.

We fitted the RACF using bi-exponential or tri-exponential functions given by the following equation:

$$y = \sum_{i=2or3} A_i \exp(-\frac{t}{\tau_i}). \quad (3)$$

Table II shows the fitting parameters for the RACF of $\hat{n}$ with a bi-exponential fitting. For $l = 1$, the slowest time scale (τ_s) is between 50 and 90 ps and the fastest time scale (τ_f) is in

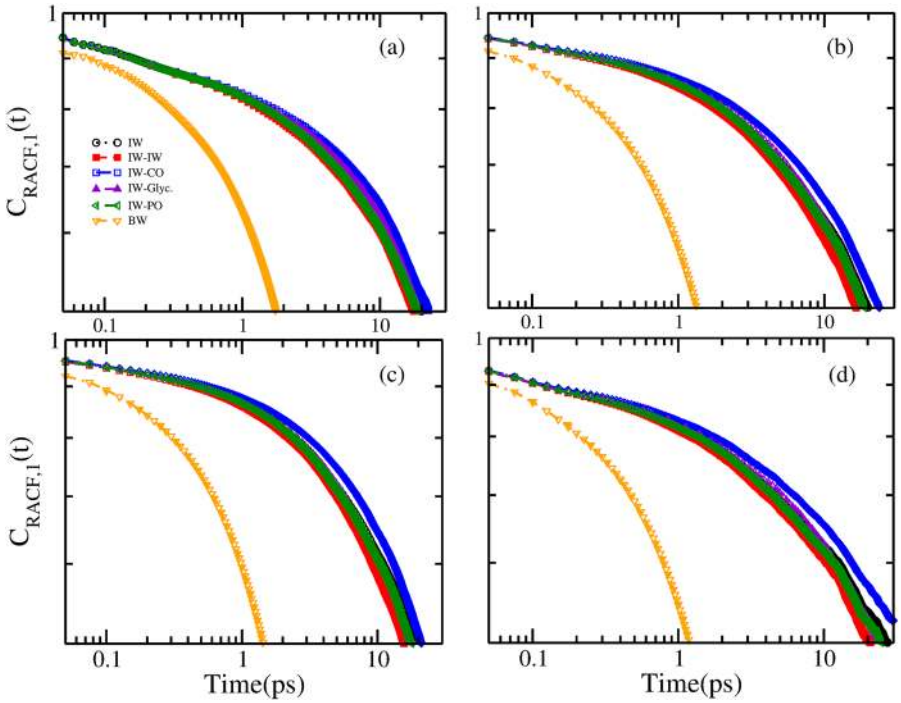

FIG. 4. RACF for interface and bulk water for l = 1 for (a) $\hat{n}$, (b) $\vec{OH}$, (c) $\vec{HH}$, and (d) $\vec{\mu}$.

the range of 2-9 ps for all the bound interfacial water. For the BW, τ_s is within 1-4 ps and τ_f is in the range of 0.2-0.4 ps. For $l = 2$, τ_s and τ_f are in between 55-78 ps and 2-3 ps, respectively, for the interfacial water, whereas these are 0.2 ps and 1.87 ps for the BW. Comparing all time scales of RACF of $l = 1$ and $l = 2$, it has been found that IW–CO obeys slower reorientation relaxation than the rest of the IW. The ratio of τ_s^1 to τ_s^2 is ≈1 for all cases indicating non-diffusive reorientation for $\hat{n}$ as found for other complex fluids.[56,57]

Table III shows the fitting parameters for the RACF of $\vec{OH}$ with a bi-exponential or tri exponential fitting from Eq. (3). For $l = 1$, τ_s and τ_f are in the range of 35-60 ps and 0.1-4 ps for the bound interfacial water and 2.4 ps and 0.2 ps, respectively, for BW. For $l = 2$, τ_s and τ_f are between 27-35 ps and 08-2 ps for all bound interfacial water and 1.16 ps and 0.14 ps for the BW. This again demonstrates the slower relaxations in the RACF for the IW–CO. The value of τ_1/τ_2 is in between 1.3 and 2 for all cases, confirming non-diffusive water reorientation for $\vec{OH}$.

Table IV shows the fitting parameters for the RACF of $\vec{HH}$ with a bi-exponential or tri-exponential function. For $l = 1$, the values of τ_s and τ_f are in the range of 35-48 ps and 0.20-4 ps,

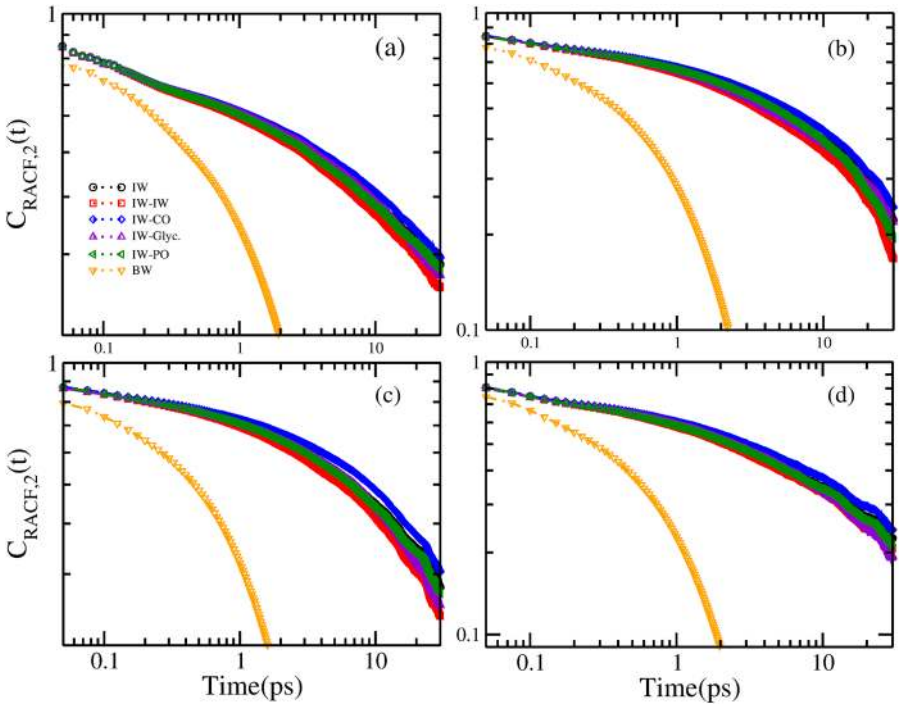

FIG. 5. RACF for interface and bulk water for l = 2 for (a) $\hat{n}$, (b) $\vec{OH}$, (c) $\vec{HH}$, and (d) $\vec{\mu}$.

TABLE II. Relaxation time scales from the fitting of the RACF for $\hat{n}$ for the interface and the bulk waters. Correlation coefficients were >0.99.

	Region	A_f	τ_f (ps)	A_s	τ_s (ps)	$\frac{\tau_1}{\tau_2}$
l = 1		0.25	6.51	0.62	83.26	
	IW					1.07
l = 2		0.29	3.05	0.42	77.83	
l = 1		0.22	5.73	0.64	65.05	
	IW–IW					1.11
l = 2		0.29	2.64	0.42	58.56	
l = 1		0.26	8.82	0.61	97.28	
	IW–CO					1.36
l = 2		0.26	3.85	0.45	71.67	
l = 1		0.19	6.13	0.68	63.55	
	IW–Glyc.					1.14
l = 2		0.26	2.67	0.46	55.92	
l = 1		0.26	6.58	0.61	83.74	
	IW–PO					1.09
l = 2		0.29	3.02	0.41	76.33	
l = 1		0.10	0.36	0.83	3.44	
	BW					1.84
l = 2		0.26	0.23	0.57	1.87	

respectively, for the bound interfacial water and 2.45 ps and 0.29 ps for the BW. For $l = 2$, τ_s and τ_f are in the range of 34-48 ps and 0.3-2.8 ps, respectively, for the interfacial water and 1.29 ps and 0.27 ps for the BW. The time scales of the RACF for $l = 1$ and $l = 2$ show slower relaxations for the IW–CO among all IWs. The value of τ_1/τ_2 is ≈1–2 for all cases demonstrating a non-diffusive behavior of $\vec{HH}$.

TABLE III. Reorientation correlation relaxation time for $\vec{OH}$ for the interface and the bulk waters. Coefficients for all classes of water were >0.99.

	Region	A_f	τ_f (ps)	A_i	τ_i (ps)	A_s	τ_s	$\frac{\tau_1}{\tau_2}$
l = 1		0.19	3.34			0.73	54.43	
	IW							1.59
l = 2		0.26	1.90			0.53	34.13	
l = 1		0.07	2.52	0.09	2.80	0.78	35.28	
	IW–IW							1.30
l = 2		0.16	0.08	0.24	1.79	0.53	27.03	
l = 1		0.17	4.22			0.74	60.16	
	IW–CO							1.72
l = 2		0.22	2.03			0.57	34.89	
l = 1		0.06	0.17	0.14	3.38	0.76	45.33	
	IW–Glyc.							1.57
l = 2		0.15	0.12	0.20	2.19	0.55	28.90	
l = 1		0.06	0.32	0.19	4.20	0.70	56.37	
	IW–PO							1.58
l = 2		0.15	0.14	0.24	2.45	0.51	35.71	
l = 1		0.06	0.26			0.87	2.41	
	BW							2.07
l = 2		0.18	0.14			0.76	1.16	

TABLE IV. Reorientation correlation relaxation time for $\vec{HH}$ for the interface and the bulk waters. Correlation coefficients for all classes of water were >0.99.

	Region	A_f	τ_i (ps)	A_i	τ_i (ps)	A_s	τ_s (ps)	$\frac{\tau_1}{\tau_2}$
l = 1		0.17	3.14			0.76	43.79	
	IW							1.00
l = 2		0.26	2.74			0.55	43.95	
l = 1		0.07	2.52	0.09	2.80	0.78	35.28	
	IW–IW							0.86
l = 2		0.15	0.61	0.22	5.01	0.49	40.92	
l = 1		0.15	3.94			0.78	47.11	
	IW–CO							1.07
l = 2		0.22	3.02			0.58	43.90	
l = 1		0.13	2.49			0.80	36.16	
	IW–Glyc.							1.05
l = 2		0.22	2.58			0.58	34.23	
l = 1		0.04	0.20	0.18	3.72	0.74	45.39	
	IW–PO							0.95
l = 2		0.13	0.34	0.24	4.06	0.51	47.40	
l = 1		0.05	0.29			0.88	2.50	
	BW							1.94
l = 2		0.17	0.17			0.69	1.29	

Table V shows the fitting parameters for the RACF of $\vec{\mu}$ with a bi-exponential or tri-exponential function. For $l = 1$, the values of τ_s and τ_f are in the range of 71-159 ps and 0.9-4 ps, respectively, for bound interfacial water and 0.18-2.24 ps for BW. For $l = 2$, τ_s and τ_f are in the range of 34-44 ps and 0.13-2.2 ps, respectively, for bound interfacial water and 0.12 ps and 1 ps for BW. Interestingly, unlike all previous cases, the time

TABLE V. Reorientation correlation relaxation time for $\vec{\mu}$ for the interface and the bulk water. Correlation coefficients for all classes of water were >0.99.

	Region	A_f	τ_f (ps)	A_i	τ_i (ps)	A_s	τ_s (ps)	$\frac{\tau_1}{\tau_2}$
l = 1		0.20	3.31			0.69	84.42	
	IW							1.88
l = 2		0.29	2.09			0.43	44.54	
l = 1		0.13	1.22	0.28	13.51	0.50	158.74	
	IW–IW							3.82
l = 2		0.19	0.22	0.24	2.94	0.41	41.55	
l = 1		0.18	3.96			0.70	96.57	
	IW–CO							2.14
l = 2		0.26	2.16			0.46	45.13	
l = 1		0.18	3.67			0.70	71.03	
	IW–Glyc.							2.04
l = 2		0.27	2.08			0.45	34.79	
l = 1		0.10	0.98	0.19	7.52	0.61	108.32	
	IW–PO							2.44
l = 2		0.21	0.13	0.26	2.66	0.41	44.37	
l = 1		0.09	0.18			0.85	2.24	
	BW							2.24
l = 2		0.22	0.12			0.59	1.00	

scales of the RACF for $l = 1$ and $l = 2$ show slower relaxations for the IW–IW among all IW. The values of τ_1/τ_2 are ≈1–2 for all cases except the IW–IW. This indicates a diffusive behavior of the RACF of $\vec{\mu}$ for IW–IW and non-diffusive behaviors for the rest of the cases.

From our analysis, we find that the RACF of the IW–CO and the IW–PO water has the most preferred orientations for most of the cases, thereby relaxing at the slowest rate among all interfacial water. In comparison to that, the orientations of the IW–IW or the IW–Glyc. have lower relaxation rates with less preferences for orientations. This is probably due to the strong electrostatic interactions between the interfacial waters and oxygen atoms of CO or PO. The trend of preferences in orientations around different chemical environments is consistent with the mosaic structure of water orientations reported earlier.[29]

D. Dynamics of hydrogen bonds

To investigate the hydrogen bond dynamics of the IW and the BW, we first identify four classes of interfacial water as described in Sec. III A. Any two IW can form hydrogen bond to each other which may not be hydrogen bonded to a third group and do not form a network. This class of water is referred to as IW. If any one of the two hydrogen bonded interface water is concertedly hydrogen bonded to another pair of hydrogen bonded interface water or to a lipid head, these are referred to as IW–IW, IW–CO, IW–Glyc., or IW–PO, respectively. The second set of hydrogen bonds can form a network structure such as IW–IW–IW–IW or lipid head-IW–IW-lipid head. The dynamics of such a hydrogen bond network between two waters are studied in this section. Since the number of water molecules in different classes of IW is different, we calculated the distribution of hydrogen bonds per water molecule for all cases. Figure 6 shows the distribution of hydrogen bonds for the interfacial water and the inset shows the distribution for the BW. The inset clearly demonstrates that the BW has nearly four hydrogen bonds per water. The numbers of hydrogen bonds are reduced in the presence of the lipid head groups in the interface. Among different classes of interfacial water molecules, the distribution of the IW–Glyc. is maximum in comparison with other classes of water. The number of hydrogen bonds per water for the IW–IW is greater than the IW–CO or the IW–Glyc. which is again greater than the IW–PO. Although, the amplitude of the distribution of hydrogen bonds in concerted networks of lipid heads–IW–IW–lipid heads is higher than that of IW–IW–IW–IW, they form a less number of hydrogen bonds compared to water in the absence of network. This is due to the annihilation of network created by hydrogen bonds in the BW due to the presence of foreign elements like DMPC head groups.[21] Thus, these networks are referred to as defected networks.

A hydrogen bond formed between one pair of donor-acceptor atoms at any time instant may not be intact at other instant. To study the dynamical behavior, we investigated mean lifetime of hydrogen bonds for all cases of waters by computing hydrogen bond auto-correlation functions (HBACFs)[58–60] defined by the following equation:

$$C_{HB}(t) = \frac{\langle h_{IW-HG}(0) h_{IW-HG}(t) \rangle}{\langle h_{IW-HG} \rangle}, \tag{4}$$

where the variable $h_{IW-HG}(t)$ represents the hydrogen bonds between interfacial water molecules (IW) and head-groups (HG) of the lipids. $h_{IW-HG}(t)$ is 1 when the water molecule forms a hydrogen bond with lipid head-groups at time t following the geometric definition mentioned in Sec. III A and is 0 otherwise. Note that the hydrogen bonds are allowed to break and thus we calculated the interrupted hydrogen bond correlation functions. Similarly, we computed the time correlation function for hydrogen bonding among the BWs as well. Figure 7 shows $C_{HB}(t)$ for the BW and all classes of IW. The HBACF for the BW decays much rapidly than the HBACF for all IW depicting a bound nature of IW as found earlier.[58,59] The hydrogen bond correlation functions of the IW–Glyc. exhibit slower decay than that of the IW–CO which is slower than the IW–IW which is again slower than that of the IW–PO. The bound water hydrogen bonded to the oxygen atoms of Glyc. is

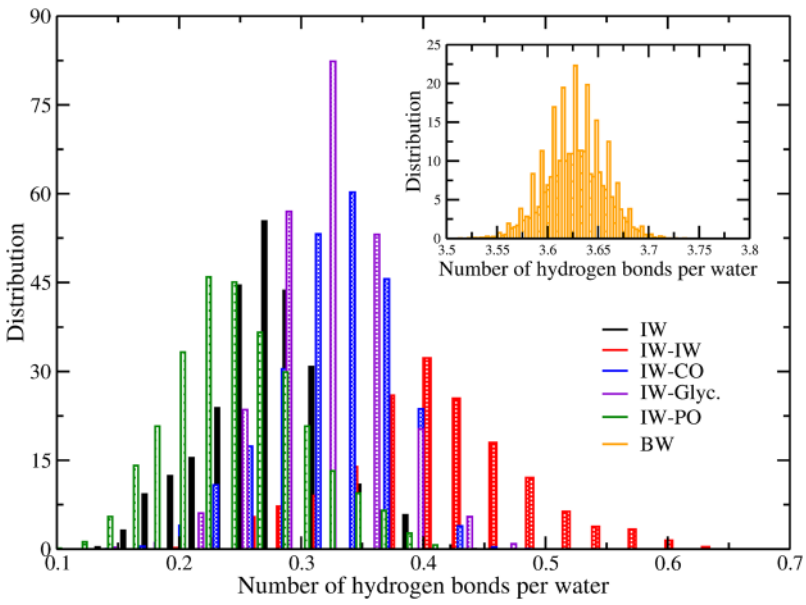

FIG. 6. Distribution of the number of hydrogen bonds per water molecule for bound interfacial waters. Inset: bulk water.

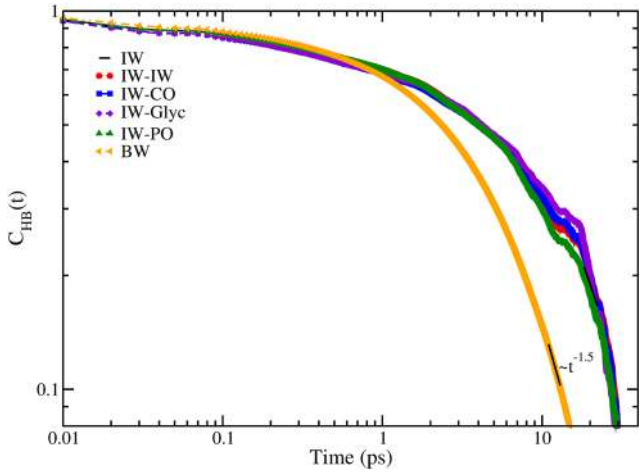

FIG. 7. Hydrogen bond auto-correlation function for interface and bulk water.

more buried in nature compared to that to the oxygen atoms of PO and thus more restricted in nature among all IW. Thus, the hydrogen bonds to Glyc. persist for a longer time span. The BW, on the other hand, has no head group influence, implying the rapid exchange of hydrogen bonds among neighbouring water molecules.

Interestingly, the hydrogen bond auto-correlation functions [$C_{HB}(t)$, in Fig. 7] of the interface water develop a hump at ~10 ps which is not observed in the BW. The humps are not found for water forming hydrogen bonds to lipid heads until the contribution of the bulk is de-constructed. Thus, the humps are consequences of the nature of chemical confinements. However, the humps disappear after ~20 ps and then all waters are found to follow a $t^{-3/2}$ asymptotic behavior. We do not report the data at longer time due to the statistical errors. The humps of the interface water are found between 12 and 20 ps which is after the onset of cage-like behavior in the MSD (Fig. 3) and before the diffusive regime of hydrogen bond break dictated by power law behavior. After the ballistic regime (>0.25 ps), chemically confined hydrogen bond networks start rattling in the cage formed by the crowded networks, and after 20 ps, water molecules succeed to leave the cage undergoing translational diffusion dictated relaxation indicated by $t^{-1.5}$ asymptotic power law irrespective of the chemical confinement. The humps of the interface water within the intermediate time scale of ~12–20 ps are possibly the signatures of a transition from motion in a cage created by chemically confined hydrogen bond networks to translational diffusions of hydrogen bonds. At longer time, the effect of chemical confinements is no longer significant and thus all classes of water irrespective of their chemical nature follow the same asymptotic behavior. The scaling parameters are clear indications that $C_{HB}(t)$ obeys the following equation:

$$C_{HB}(t) \approx \frac{1}{4\pi D t^{1.5}}, \tag{5}$$

where D is the diffusion constant at longer time. Thus, irrespective of the nature of the chemical confinement of IW and BW, the hydrogen bond breaking and formation mechanism is found to be dictated by the translational diffusion in three dimensions.[61]

Kinetics of hydrogen bonding formation and breaking are studied using the reactive flux analysis[25,51,62] where the forward rate constant (k) and backward rate constant (k') are considered for the hydrogen bond breaking and formation, respectively,

$$K(t) = -\frac{dC_{HB}(t)}{dt} \tag{6}$$

and

$$K(t) = kC_{HB}(t) - k'n(t). \tag{7}$$

Here, $n(t)$ represents the probability that a hydrogen bond existed at time $t = 0$ but the two atoms which are forming hydrogen bonds are still within the distance cutoff. The lifetime for hydrogen bonding can be computed using the forward rate constant as

$$\tau = \frac{1}{k}. \tag{8}$$

Assuming the process of hydrogen bond breaking as the Eyring process, one can find the Gibbs energy ($\Delta G^{\ddagger}$) of the hydrogen bond breaking activation using the following relation:

$$\tau = \frac{h}{k_B T} e^{\frac{\Delta G^{\ddagger}}{k_B T}}, \tag{9}$$

where k_B is Boltzmann's constant, T is the temperature, and h is Planck's constant. The bulk water has no influence of lipids; thus two water molecules hydrogen bonded tend to break at a shorter period of time and have shorter lifetime than the IW. Thus the BW has lower $\Delta G^{\ddagger}$ than all IW. The value of $\Delta G^{\ddagger}$ for TIP4P/2005 bulk water is found to be 8.29 kJ mol^{-1} which is somewhat higher than the values reported for bulk water of TIP4P or SPC/E.[25] The difference is attributed to the slower diffusion of the TIP4P/2005 water model than that of TIP4P or SPC/E[33] bulk water leading to an energy cost in the hydrogen bond exchange mechanism. Bound water hydrogen bonded to lipid head groups stays bonded for a longer period of time. Interestingly, the values of $\Delta G^{\ddagger}$ decrease from IW–Glyc. to IW–CO, to IW–IW, to IW–PO (Table VI). The trend of lowering in $\Delta G^{\ddagger}$ indicates the importance of location of DMPC head groups on the activation energy of hydrogen bond breakage. Since the IW–Glyc. is more buried into the hydrophobic region of the bilayer due to the location of Glyc. oxygen along the alkyl chains, diffusion of IW–Glyc. while hydrogen bond exchange or reshuffling through the water depleted hydrophobic environment requires more energy of activation cost. Thus, the interfacial water hydrogen bonded to Glyc. oxygen shows more trapped behavior compared to the ones for the CO or the PO. The confined and buried Glyc. head groups may disrupt the necessary pathways for hydrogen bond exchange. This information indicates that the contribution of hydrogen bond

TABLE VI. Hydrogen bond lifetime and Gibbs energy of activation for interface and bulk waters.

Region	τ (ps)	$\Delta G^{\ddagger}$ (kJ mol^{-1})
IW–IW	14.96	11.69
IW–CO	16.74	11.98
IW–Glyc.	18.96	12.30
IW–PO	13.00	11.33
BW	3.98	8.29

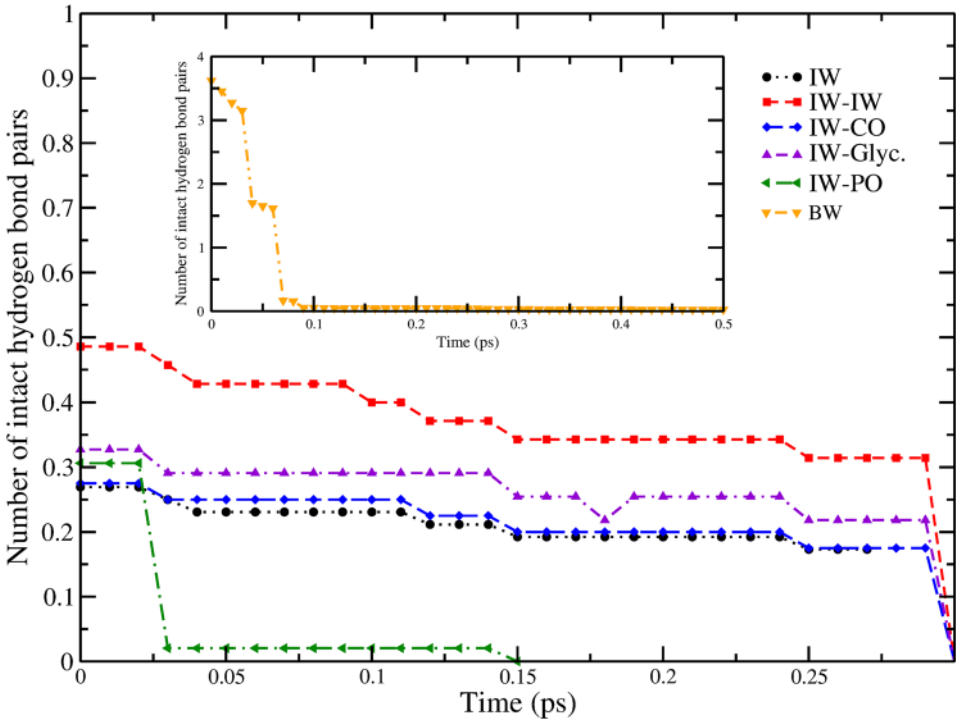

FIG. 8. Number of hydrogen bonds per water molecule which remain *intact* for simulation time t are shown for interfacial water. Inset: bulk water.

networks on the changes in Gibbs free energy and on the thermodynamic stability of lipid bilayers needs further attention which can be investigated by calculating changes in enthalpy and entropy on breaking of hydrogen bonds in future. Thus the present calculations explain the role of chemical confinement on breaking of defected networks as well as lay a foundation for future work which further may shed light on the connection of thermodynamics of hydrogen bonds to their dynamics and enhance our understanding on the stability of other biomolecules like proteins.[63,64]

E. Hydrogen bond networks and lipid-lipid associations

In order to find the influence of the hydrogen bond dynamics on the membrane structure, the IW–IW, the IW–CO, the IW–PO, and the IW–Glyc. water molecules which remain *continuously* hydrogen bonded among themselves during simulation time are identified. These hydrogen bonds remain *intact* without allowing changes in their respective donor acceptor partners. However, the other hydrogen bonds to the lipid heads in the network are allowed to diffuse. Figure 8 shows the number of hydrogen bonds per water which are *intact* during simulation time. The inset shows the number of *intact* hydrogen bonds per water for the BW. The numbers of the BW are higher than the remaining classes of water which is in agreement with the distribution of number of hydrogen bonds per water molecule shown in the inset of Fig. 6. Interestingly, the number of intact hydrogen bonds for the BW decreases sharply and faster than that for any IW. The number of hydrogen bonds for the IW–PO decreases faster than the rest of the IW. The time evolution of all *intact* hydrogen bonds indicates toward their lifetime without the information of pair diffusion. They follow similar trends as the lifetime of hydrogen bonds when pair diffusion is allowed (see Table VI). Importantly, the time evolution of *intact* hydrogen bonds refer to the lifetime of defected hydrogen bond networks formed between lipid head groups and interfacial water. The defected network by the IW–PO breaks faster than that by the IW–CO or the IW–Glyc. since the IW–CO or the IW–Glyc. is more buried in the core hydrophobic region of lipids. So the hydrogen bonds near lipid tails remain intact for longer time due to the association of dense lipid tails. Figure 9 shows a snapshot of hydrogen bond networks where IW is hydrogen bonded to IW and concertedly hydrogen bonded to CO, Glyc., or PO of lipids resulting in water mediated associations of lipids.

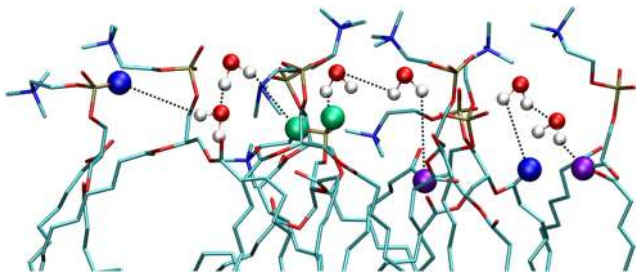

FIG. 9. Snapshot of DMPC molecules hydrogen bonded to interfacial TIP4P/2005 water.[53] DMPC and water are shown in licorice and Corey, Pauling, and Koltun representations, respectively. Hydrogen bonded oxygens of DMPC are shown in VDW representations. Color code: green—PO oxygen, violet—Glyc. oxygen, blue—CO oxygen, red—water oxygen.

IV. CONCLUSION

Continuously residing interfacial water molecules in hydrated DMPC lipid bilayer are identified to form hydrogen bonds among themselves and concertedly to the oxygens of CO, PO, or Glyc. of DMPC heads. Radial distribution functions of interface water oxygens are found to have higher amplitudes compared to that of the bulk due to the more tendency of oxygens to be in the nearest neighbors of each other

in the presence of lipid heads. This consequently disrupts the tetrahedral network in bulk water and leads to defects in the networks of interface water. Mean square displacements of all classes of interface water show signatures of cage-like and glass-like regions for a short duration of time after the ballistic regions followed by sub-diffusive regions. The nature of chemical confinement is found to be important to translational dynamics since the MSD of the IW–CO is slower than the IW–Glyc. which is slower than the IW–PO or the IW–IW. The first and second order RACFs are computed for $\vec{n}$ ($\vec{\mathrm{OH}} \times \vec{\mathrm{HH}}$), $\vec{\mathrm{OH}}$, $\vec{\mathrm{HH}}$, and $\vec{\mu}$. In all cases, the RACF of the BW decays faster compared to all classes of IW. The IW–CO and the IW–PO are found to have higher preferences in orientations, whereas the IW–Glyc. or the IW–IW has lower preferences. This is consistent with the mosaic structure in the orientation of IW near DMPC reported earlier.[29] The ratio of the first and the second order Legendre polynomial of the RACF for all water hydrogen bonded to lipid heads indicates the presence of the jump reorientation mechanism during hydrogen bond switching events. Although the number of hydrogen bonds for the IW is lower than that for the BW due to the defected hydrogen bond network in the presence of the lipid heads, the amplitude of distribution of hydrogen bonds is higher for the IW than that for the BW. Hydrogen bond correlation functions for the BW decay much faster than all IW. The IW–PO exhibits faster decay in hydrogen bond correlation than the IW–IW which decays faster than the IW–CO or the IW–Glyc. This is due to their locations along the alkyl chains in membranes. Interestingly, hydrogen bond auto-correlation functions for interface water develop humps at ∼12 ps after the onset of glass-like behavior which is neither present in bulk nor in water hydrogen bonded to lipid heads. The humps disappear at longer time due to the escape of water molecules from the cage of the crowded networks when the effect of confinement is no longer significant and thus all classes of water follow a $t^{-3/2}$ behavior delineating the translational diffusion dictated hydrogen bond dynamics irrespective of the nature of the chemical confinement of water. In the intermediate time scale of ∼12–20 ps, the interface water undergoes a transition from the glass-like behavior to the diffusion dictated hydrogen bond breakage mechanism leading to humps in the correlation functions. Using the reactive flux analysis, the Gibbs energy of activation of hydrogen bond breakage is calculated. The BW has the smallest lifetime with the lowest Gibbs energy of activation, whereas the IW–Glyc. has the longest lifetime with the highest Gibbs energy of activation among all water. Since IW–Glyc. is buried in the core lipid regime, diffusion through the water depleted hydrophobic environment is not favourable leading to a high Gibbs energy of activation. However, the relation of thermodynamics to the dynamics of hydrogen bond can only be found once the changes in entropy and enthalpy are calculated. This can establish the contribution of hydrogen bonding relaxation to thermodynamic or kinetic stability of lipid aggregations in the future. Our calculations show that the hydrogen bond networks which remain *intact* during the simulation time decay much rapidly for the BW than all defected hydrogen bond networks in the interface. The defected hydrogen bond networks dynamically result in the water mediated lipid-lipid associations. Thus, the present work enhances our understanding on slower hydration dynamics of membranes due to the chemical nature of hydrogen bond networks. This can be useful for further investigations on the dynamics of proton migrations from the hydration layer of membranes to the bulk phase or toward the stability of membranes or other biomolecules like proteins.[63–68]

ACKNOWLEDGMENTS

A.D. is thankful to SERB (Project No. SB/FT/CS-134/2013) for funding.

[1] P. Jungwirth, "Biological water or rather water in biology?," J. Phys. Chem. Lett. **6**(13), 2449–2451 (2015).
[2] N. Nandi and B. Bagchi, "Dielectric relaxation of biological water," J. Phys. Chem. B **101**(50), 10954–10961 (1997).
[3] J. Milhaud, "New insights into water–phospholipid model membrane interactions," Biochim. Biophys. Acta, Biomembr. **1663**(1-2), 19–51 (2004).
[4] G. Hummer and A. Tokmakoff, "Preface: Special topic on biological water," J. Chem. Phys. **141**(22), 22D101 (2014).
[5] S. M. Gruenbaum and J. L. Skinner, "Vibrational spectroscopy of water in hydrated lipid multi-bilayers. III. Water clustering and vibrational energy transfer," J. Chem. Phys. **139**(17), 175103 (2013).
[6] S. Woutersen and H. J. Bakker, "Resonant intermolecular transfer of vibrational energy in liquid water," Nature **402**, 507–509 (1999).
[7] N. Huse, J. R. Dwyer, B. Chugh, E. T. J. Nibbering, T. Elsaesser, R. J. D. Miller, M. L. Cowan, and B. D. Bruner, "Ultrafast memory loss and energy redistribution in the hydrogen bond network of liquid H_2O," Nature **434**, 199–202 (2005).
[8] M. Ji, M. Odelius, and K. J. Gaffney, "Large angular jump mechanism observed for hydrogen bond exchange in aqueous perchlorate solution," Science **328**(5981), 1003–1005 (2010).
[9] S. Woutersen, U. Emmerichs, and H. J. Bakker, "Femtosecond mid-IR pump-probe spectroscopy of liquid water: Evidence for a two-component structure," Science **278**(5338), 658–660 (1997).
[10] H.-K. Nienhuys, R. A. van Santen, and H. J. Bakker, "Orientational relaxation of liquid water molecules as an activated process," J. Chem. Phys. **112**(19), 8487–8494 (2000).
[11] G. Gallot, S. Bratos, S. Pommeret, N. Lascoux, J.-C. Leicknam, M. Koziński, W. Amir, and G. M. Gale, "Coupling between molecular rotations and OH$\cdots$O motions in liquid water: Theory and experiment," J. Chem. Phys. **117**(24), 11301–11309 (2002).
[12] D. Laage, G. Stirnemann, F. Sterpone, R. Rey, and J. T. Hynes, "Reorientation and allied dynamics in water and aqueous solutions," Annu. Rev. Phys. Chem. **62**(1), 395–416 (2011).
[13] J. Teixeira, M. C. Bellissent-Funel, S. H. Chen, and A. J. Dianoux, "Experimental determination of the nature of diffusive motions of water molecules at low temperatures," Phys. Rev. A **31**, 1913–1917 (1985).
[14] D. Russo, R. K. Murarka, J. R. D. Copley, and T. Head-Gordon, "Molecular view of water dynamics near model peptides," J. Phys. Chem. B **109**(26), 12966–12975 (2005).
[15] D. Di Cola, A. Deriu, M. Sampoli, and A. Torcini, "Proton dynamics in supercooled water by molecular dynamics simulations and quasielastic neutron scattering," J. Chem. Phys. **104**(11), 4223–4232 (1996).
[16] A. Faraone, L. Liu, and S.-H. Chen, "Model for the translation–rotation coupling of molecular motion in water," J. Chem. Phys. **119**(12), 6302–6313 (2003).
[17] J. Jonas, T. DeFries, and D. J. Wilbur, "Molecular motions in compressed liquid water," J. Chem. Phys. **65**(2), 582–588 (1976).
[18] J. Qvist and B. Halle, "Thermal signature of hydrophobic hydration dynamics," J. Am. Chem. Soc. **130**(31), 10345–10353 (2008).
[19] J. Ropp, C. Lawrence, T. C. Farrar, and J. L. Skinner, "Rotational motion in liquid water is anisotropic: A nuclear magnetic resonance and molecular dynamics simulation study," J. Am. Chem. Soc. **123**(33), 8047–8052 (2001).
[20] P. B. Moore, C. F. Lopez, and M. L. Klein, "Dynamical properties of a hydrated lipid bilayer from a multinanosecond molecular dynamics simulation," Biophys. J. **81**(5), 2484–2494 (2001).
[21] M. Pasenkiewicz-Gierula, Y. Takaoka, H. Miyagawa, K. Kitamura, and A. Kusumi, "Charge pairing of headgroups in phosphatidylcholine membranes: A molecular dynamics simulation study," Biophys. J. **76**(3), 1228–1240 (1999).

[22]A. M. Smondyrev and G. A. Voth, "Molecular dynamics simulation of proton transport near the surface of a phospholipid membrane," Biophys. J. **82**(3), 1460–1468 (2002).
[23]P. M. Kasson and V. S. Pande, "Molecular dynamics simulation of lipid reorientation at bilayer edges," Biophys. J. **86**(6), 3744–3749 (2004).
[24]L. Sapir and D. Harries, "Revisiting hydrogen bond thermodynamics in molecular simulations," J. Chem. Theory Comput. **13**(6), 2851–2857 (2017).
[25]D. van der Spoel, P. J. van Maaren, P. Larsson, and N. Tîmneanu, "Thermodynamics of hydrogen bonding in hydrophilic and hydrophobic media," J. Phys. Chem. B **110**(9), 4393–4398 (2006).
[26]O. Fisette, C. Päslack, R. Barnes, J. Mario Isas, R. Langen, M. Heyden, S. Han, and L. V. Schäfer, "Hydration dynamics of a peripheral membrane protein," J. Am. Chem. Soc. **138**(36), 11526–11535 (2016).
[27]J. M. Franck, Y. Ding, K. Stone, P. Z. Qin, and S. Han, "Anomalously rapid hydration water diffusion dynamics near DNA surfaces," J. Am. Chem. Soc. **137**(37), 12013–12023 (2015).
[28]R. Biswas, J. Furtado, and B. Bagchi, "Layerwise decomposition of water dynamics in reverse micelles: A simulation study of two-dimensional infrared spectrum," J. Chem. Phys. **139**(14), 144906 (2013).
[29]S. Re, W. Nishima, T. Tahara, and Y. Sugita, "Mosaic of water orientation structures at a neutral zwitterionic lipid/water interface revealed by molecular dynamics simulations," J. Phys. Chem. Lett. **5**(24), 4343–4348 (2014).
[30]A. Kundu, K. Kwak, and M. Cho, "Water structure at the lipid multibilayer surface: Anionic versus cationic head group effects," J. Phys. Chem. B **120**(22), 5002–5007 (2016).
[31]T. Ohto, E. H. G. Backus, C.-S. Hsieh, M. Sulpizi, M. Bonn, and Y. Nagata, "Lipid carbonyl groups terminate the hydrogen bond network of membrane-bound water," J. Phys. Chem. Lett. **6**(22), 4499–4503 (2015).
[32]C. F. Lopez, S. O. Nielsen, M. L. Klein, and P. B. Moore, "Hydrogen bonding structure and dynamics of water at the dimyristoylphosphatidylcholine lipid bilayer surface from a molecular dynamics simulation," J. Phys. Chem. B **108**(21), 6603–6610 (2004).
[33]J. L. F. Abascal and C. Vega, "A general purpose model for the condensed phases of water: TIP4P/2005," J. Chem. Phys. **123**(23), 234505 (2005).
[34]O. Berger, O. Edholm, and F. Jähnig, "Molecular dynamics simulations of a fluid bilayer of dipalmitoylphosphatidylcholine at full hydration, constant pressure, and constant temperature," Biophys. J. **72**(5), 2002–2013 (1997).
[35]A. Cordomí, G. Caltabiano, and L. Pardo, "Membrane protein simulations using AMBER force field and Berger lipid parameters," J. Chem. Theory Comput. **8**(3), 948–958 (2012).
[36]H. J. C. Berendsen, J. P. M. Postma, W. F. van Gunsteren, A. DiNola, and J. R. Haak, "Molecular dynamics with coupling to an external bath," J. Chem. Phys. **81**(8), 3684–3690 (1984).
[37]U. Essmann, L. Perera, M. L. Berkowitz, T. Darden, H. Lee, and L. G. Pedersen, "A smooth particle mesh Ewald method," J. Chem. Phys. **103**(19), 8577–8593 (1995).
[38]D. J. Tildesley and M. P. Allen, *Computer Simulations of Liquids* (Oxford University Press, New York, 1987).
[39]T. Darden, D. York, and L. Pedersen, "Particle mesh Ewald: An $N\cdot\log(N)$ method for Ewald sums in large systems," J. Chem. Phys. **98**(12), 10089–10092 (1993).
[40]H. Bekker, H. J. C. Berendsen, E. J. Dijkstra, S. Achterop, R. Vondrumen, D. van der Spoel, A. Sijbers, H. Keegstra, and M. K. R. Renardus, "Gromacs—A parallel computer for molecular-dynamics simulations," in *Physics Computing '92*, edited by R. A. DeGroot and J. Nadrchal (World Scientific Publishing, 1993), pp. 252–256.
[41]H. J. C. Berendsen, D. van der Spoel, and R. van Drunen, "Gromacs: A message-passing parallel molecular-dynamics implementation," Comput. Phys. Commun. **91**(1-3), 43–56 (1995).
[42]E. Lindahl, B. Hess, and D. van der Spoel, "Gromacs 3.0: A package for molecular simulation and trajectory analysis," Mol. Modell. Annu. **7**(8), 306–317 (2001).
[43]D. van der Spoel, E. Lindahl, B. Hess, G. Groenhof, A. E. Mark, and H. J. C. Berendsen, "Gromacs: Fast, flexible, and free," J. Comput. Chem. **26**(16), 1701–1718 (2005).
[44]B. Hess, C. Kutzner, D. van der Spoel, and E. Lindahl, "Gromacs 4: Algorithms for highly efficient, load-balanced, and scalable molecular simulation," J. Chem. Theory Comput. **4**(3), 435–447 (2008).
[45]D. van der Spoel, E. Lindahl, B. Hess, and the GROMAC development team, GOMACS User Manual version 4.6.5, www.gromacs.org (2013).
[46]A. Debnath, B. Mukherjee, K. G. Ayappa, P. K. Maiti, and S.-T. Lin, "Entropy and dynamics of water in hydration layers of a bilayer," J. Chem. Phys. **133**(17), 174704 (2010).
[47]A. Debnath, K. G. Ayappa, and P. K. Maiti, "Simulation of influence of bilayer melting on dynamics and thermodynamics of interfacial water," Phys. Rev. Lett. **110**, 018303 (2013).
[48]R. Rey, K. B. Møller, and J. T. Hynes, "Hydrogen bond dynamics in water and ultrafast infrared spectroscopy," J. Phys. Chem. A **106**(50), 11993–11996 (2002).
[49]C. P. Lawrence and J. L. Skinner, "Vibrational spectroscopy of HOD in liquid D_2O. III. Spectral diffusion, and hydrogen-bonding and rotational dynamics," J. Chem. Phys. **118**(1), 264–272 (2003).
[50]J. D. Eaves, J. J. Loparo, C. J. Fecko, S. T. Roberts, A. Tokmakoff, and P. L. Geissler, "Hydrogen bonds in liquid water are broken only fleetingly," Proc. Natl. Acad. Sci. U. S. A. **102**, 13019 (2005).
[51]A. Luzar and D. Chandler, "Hydrogen-bond kinetics in liquid water," Nature **379**, 55–57 (1996).
[52]L. Bosio, S. Hsin Chen, and J. Teixeira, "Isochoric temperature differential of the x-ray structure factor and structural rearrangements in low-temperature heavy water," Phys. Rev. A **27**, 1468–1475 (1983).
[53]W. Humphrey, A. Dalke, and K. Schulten, "VMD—Visual molecular dynamics," J. Mol. Graphics **14**, 33–38 (1996).
[54]J. Swenson, F. Kargl, P. Berntsen, and C. Svanberg, "Solvent and lipid dynamics of hydrated lipid bilayers by incoherent quasielastic neutron scattering," J. Chem. Phys. **129**(4), 045101 (2008).
[55]C. Vega, J. L. F. Abascal, M. M. Conde, and J. L. Aragones, "What ice can teach us about water interactions: A critical comparison of the performance of different water models," Faraday Discuss. **141**, 251–276 (2009).
[56]S. Das, R. Biswas, and B. Mukherjee, "Reorientational jump dynamics and its connections to hydrogen bond relaxation in molten acetamide: An all-atom molecular dynamics simulation study," J. Phys. Chem. B **119**(1), 274–283 (2015).
[57]A. C. Fogarty and D. Laage, "Water dynamics in protein hydration shells: The molecular origins of the dynamical perturbation," J. Phys. Chem. B **118**(28), 7715–7729 (2014).
[58]A. Luzar and D. Chandler, "Effect of environment on hydrogen bond dynamics in liquid water," Phys. Rev. Lett. **76**, 928–931 (1996).
[59]A. Chandra, "Effects of ion atmosphere on hydrogen-bond dynamics in aqueous electrolyte solutions," Phys. Rev. Lett. **85**, 768–771 (2000).
[60]S. Balasubramanian, S. Pal, and B. Bagchi, "Hydrogen-bond dynamics near a micellar surface: Origin of the universal slow relaxation at complex aqueous interfaces," Phys. Rev. Lett. **89**, 115505 (2002).
[61]O. Markovitch and N. Agmon, "Reversible geminate recombination of hydrogen-bonded water molecule pair," J. Chem. Phys. **129**(8), 084505 (2008).
[62]A. Luzar, "Resolving the hydrogen bond dynamics conundrum," J. Chem. Phys. **113**(23), 10663–10675 (2000).
[63]A. V. Efimov and E. V. Brazhnikov, "Relationship between intramolecular hydrogen bonding and solvent accessibility of side-chain donors and acceptors in proteins," FEBS Lett. **554**(3), 389–393 (2003).
[64]K. A. Dill, "Dominant forces in protein folding," Biochemistry **29**(31), 7133–7155 (1990).
[65]B. Gabriel and J. Teissié, "Proton long-range migration along protein monolayers and its consequences on membrane coupling," Proc. Natl. Acad. Sci. U. S. A. **93**, 14521 (1996).
[66]A. M. Smondyrev and G. A. Voth, "Molecular dynamics simulation of proton transport through the influenza a virus M2 channel," Biophys. J. **83**(4), 1987–1996 (2002).
[67]H. L. Tepper and G. A. Voth, "Protons may leak through pure lipid bilayers via a concerted mechanism," Biophys. J. **88**(5), 3095–3108 (2005).
[68]M. E. Tuckerman, D. Marx, M. L. Klein, and M. Parrinello, "On the quantum nature of the shared proton in hydrogen bonds," Science **275**(5301), 817–820 (1997).